

Proceedings of the Institution of Mechanical Engineers, Part G: Journal of Aerospace Engineering

<http://pig.sagepub.com/>

Combining experimental data, computational fluid dynamics, and six-degree of freedom simulation to develop a guidance actuator for a supersonic projectile

K C Massey and S I Silton

Proceedings of the Institution of Mechanical Engineers, Part G: Journal of Aerospace Engineering 2009 223: 341

DOI: 10.1243/09544100JAERO399

The online version of this article can be found at:
<http://pig.sagepub.com/content/223/4/341>

Published by:



<http://www.sagepublications.com>

On behalf of:



[Institution of Mechanical Engineers](http://www.imech.org)

Additional services and information for *Proceedings of the Institution of Mechanical Engineers, Part G: Journal of Aerospace Engineering* can be found at:

Email Alerts: <http://pig.sagepub.com/cgi/alerts>

Subscriptions: <http://pig.sagepub.com/subscriptions>

Reprints: <http://www.sagepub.com/journalsReprints.nav>

Permissions: <http://www.sagepub.com/journalsPermissions.nav>

Citations: <http://pig.sagepub.com/content/223/4/341.refs.html>

Report Documentation Page

Form Approved
OMB No. 0704-0188

Public reporting burden for the collection of information is estimated to average 1 hour per response, including the time for reviewing instructions, searching existing data sources, gathering and maintaining the data needed, and completing and reviewing the collection of information. Send comments regarding this burden estimate or any other aspect of this collection of information, including suggestions for reducing this burden, to Washington Headquarters Services, Directorate for Information Operations and Reports, 1215 Jefferson Davis Highway, Suite 1204, Arlington VA 22202-4302. Respondents should be aware that notwithstanding any other provision of law, no person shall be subject to a penalty for failing to comply with a collection of information if it does not display a currently valid OMB control number.

1. REPORT DATE 11 NOV 2008		2. REPORT TYPE		3. DATES COVERED 00-00-2008 to 00-00-2008	
4. TITLE AND SUBTITLE Combining Experimental Data, Computational Fluid Dynamics, And Six-Degree Of Freedom Simulation To Develop A Guidance Actuator For A Supersonic Projectile				5a. CONTRACT NUMBER	
				5b. GRANT NUMBER	
				5c. PROGRAM ELEMENT NUMBER	
6. AUTHOR(S)				5d. PROJECT NUMBER	
				5e. TASK NUMBER	
				5f. WORK UNIT NUMBER	
7. PERFORMING ORGANIZATION NAME(S) AND ADDRESS(ES) Army Research Laboratory, Weapons and Materials Research Directorate, Aberdeen Proving Ground, MD, 20783				8. PERFORMING ORGANIZATION REPORT NUMBER	
9. SPONSORING/MONITORING AGENCY NAME(S) AND ADDRESS(ES)				10. SPONSOR/MONITOR'S ACRONYM(S)	
				11. SPONSOR/MONITOR'S REPORT NUMBER(S)	
12. DISTRIBUTION/AVAILABILITY STATEMENT Approved for public release; distribution unlimited					
13. SUPPLEMENTARY NOTES Proceedings of the Institution of Mechanical Engineers, Part G: Journal of Aerospace Engineering 2009					
14. ABSTRACT A joint effort between the Georgia Tech Research Institute and the Army Research Lab successfully used a combination of numerical and experimental results to demonstrate the performance of a guidance actuator for a supersonic projectile. The use of computational and experimental approaches greatly enhanced the understanding of how the actuators worked as well enabled the program to be completed for a lower cost than if either the modelling or the experiments had been neglected. Wind tunnel experiments were used with computational fluid dynamics results to provide aerodynamic coefficients for six-degree of freedom (6-DOF) simulations. The 6-DOF simulations were used to predict the performance of the projectile in the range, thus ensuring that good range data were acquired and reducing the necessary number of set-up rounds. It was found that there were cases where experimental methods were necessary, although the modelling provided the researchers with a greater detail of flow interactions and provided forces that were difficult to measure.					
15. SUBJECT TERMS					
16. SECURITY CLASSIFICATION OF:			17. LIMITATION OF ABSTRACT	18. NUMBER OF PAGES	19a. NAME OF RESPONSIBLE PERSON
a. REPORT unclassified	b. ABSTRACT unclassified	c. THIS PAGE unclassified			

Combining experimental data, computational fluid dynamics, and six-degree of freedom simulation to develop a guidance actuator for a supersonic projectile

K C Massey^{1*} and S I Silton²

¹Aerospace, Transportation, and Advanced Systems Laboratory, Georgia Tech Research Institute, Atlanta, Georgia, USA

²Weapons and Materials Research Directorate, Army Research Laboratory, Aberdeen Proving Ground, Maryland, USA

The manuscript was received on 20 June 2008 and was accepted after revision for publication on 11 November 2008.

DOI: 10.1243/09544100JAERO399

Abstract: A joint effort between the Georgia Tech Research Institute and the Army Research Lab successfully used a combination of numerical and experimental results to demonstrate the performance of a guidance actuator for a supersonic projectile. The use of computational and experimental approaches greatly enhanced the understanding of how the actuators worked as well enabled the program to be completed for a lower cost than if either the modelling or the experiments had been neglected. Wind tunnel experiments were used with computational fluid dynamics results to provide aerodynamic coefficients for six-degree of freedom (6-DOF) simulations. The 6-DOF simulations were used to predict the performance of the projectile in the range, thus ensuring that good range data were acquired and reducing the necessary number of set-up rounds. It was found that there were cases where experimental methods were necessary, although the modelling provided the researchers with a greater detail of flow interactions and provided forces that were difficult to measure.

Keywords: guided projectile, guided munition, guided bullet, smart projectile, smart bullet, smart projectile, flow control, 6-DOF, RAM defence, range test

1 INTRODUCTION

There has been a recent interest in both missiles and guided projectiles that operate in the high-supersonic to hypersonic range for various missions. The Office of Naval Research has been pursuing HyFly [1] since early 2002. HyFly is a proposed Mach 6 missile that would be used to strike targets of opportunity in a timely fashion before they could reposition. Another area of interest revolves around defending against threats with small radar cross-sections that cannot be engaged at long ranges due to problems with detecting them. These threats include small objects such as mortars and rockets as well as stealthy larger targets such as cruise missiles. The enhanced area protection system under development by the Army [2] is pursuing a technology that will enable ground-based defence against such

threats. One possible scheme for defence against these threats assumes that medium-caliber guns with high rates of fire would fire multiple supersonic projectiles that could be guided into the threat [3]. The course corrections would greatly enhance the hit probability of a single round and thus expand the area defended by a single gun. Warnash and Killen [4] describe several military programs where high-speed guided munitions are under consideration or in development. In all cases, it is found that the high closure rates between the projectile and the target may necessitate large turning forces.

Although several years of experimental [5] and computational [6] research have indicated that a supersonic projectile could be manoeuvred with guidance pins, this technology had not been demonstrated on an actual gun-launched projectile. Thus, the main goal of this effort was to demonstrate that a gun-fired supersonic projectile could be manoeuvred with the previously developed guidance pins. It was also desired to quantify the aerodynamic forces developed on an actual projectile in supersonic

*Corresponding author: ATAS, Georgia Tech Research Institute, 7220 Richardson Road, Smyrna, Georgia 30080, USA.
email: kevin.massey@gtri.gatech.edu

flight in order to validate both the computational fluid dynamics (CFD) and the six-degree of freedom (6-DOF) models at full scale and full velocity. With the limited amounts of funds available, it was necessary to maximize the data acquired from the single use test rounds. The goal was to use a combined experimental and computational approach to predict the aerodynamic performance of the rounds and thus their trajectory, thereby allowing the expensive range tests to be used to validate the predictions as opposed to determining the aerodynamic coefficients directly, which would require a larger number of test fires.

2 PIN FIN CONCEPT AND EXPERIMENTAL EVALUATION

Building on the fact that the flow disturbance introduced by a jet or solid object inserted into the flow is three dimensional in nature and extends away from the body of the projectile, it was hypothesized that if the actuator was moved close to a fin, there would be regions of high pressure generated not only on the body but also on the fin. This concept is shown conceptually in Fig. 1 where a shock is created by an interaction between two pins and the flow. In this conceptual image, the shock also has a large interaction with the fin as well as the body. However, because of the placement of the two pins between consecutive fins, the forces of the fins cancel (i.e. no roll), while the body forces are additive. Taking advantage of this three-dimensional corner effect should enlarge the surface area of the projectile experiencing high pressure relative to positioning the actuator further away from the fins. One advantage of this concept is the fact that generating forces on the surfaces of the fins allows one to also control the roll rate of the projectile or missile if the pins are placed in diametric opposition – the body forces cancel, while the forces on the fins are additive allowing roll control. This enables the pursuit of different control schemes that might not have otherwise been possible.

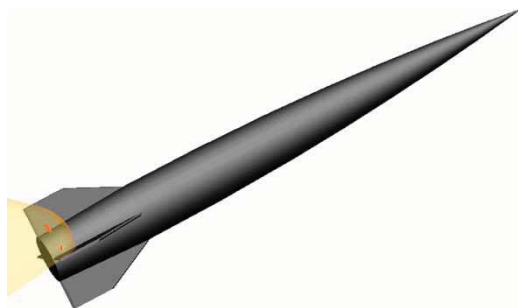


Fig. 1 Pin fin concept

2.1 Test set-up

To validate this concept, a series of experimental tests were conducted. The first experimental tests used a simplified representative geometry that consisted of a fin on a flat plate immersed in a supersonic stream. The jet was a convergent divergent jet that could be operated at Mach 1.7 in a nearly shock-free fashion. The fin was mounted onto a disc that could be rotated to change the angle of attack of the fin relative to the stream. A picture of this hardware mounted onto GTRI's Hot Jet Facility is shown in Fig. 2. The fin was designed to maximize its size while still allowing it to be immersed in the jet; it was 1.5 in tall and 3 in long. The fin was instrumented with 28 pressure taps that were cut into the fin using a wire electrical discharge machining process. The pressure port locations are shown in Fig. 3, where the areas used for the force calculations are also shown. The pressures measured from these pressure ports were used to estimate the force on the fin by assuming a constant pressure in the vicinity of the pressure ports. Pressure contours were also created using Tecplot, where the contours were based on the standard Tecplot methodologies of triangulation and linear interpolation. Adjacent to the fin was located a series of blocks into which various

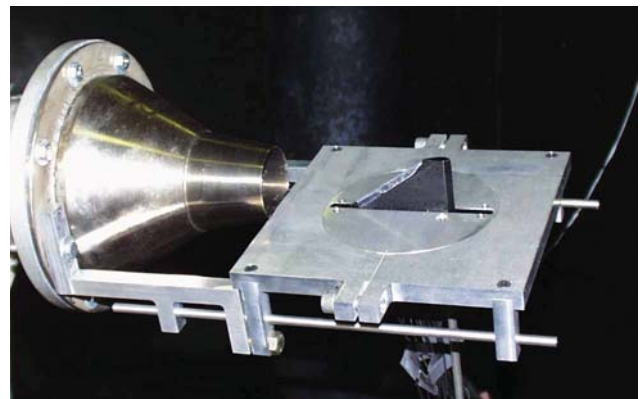


Fig. 2 Installed hardware of fin interaction experiment

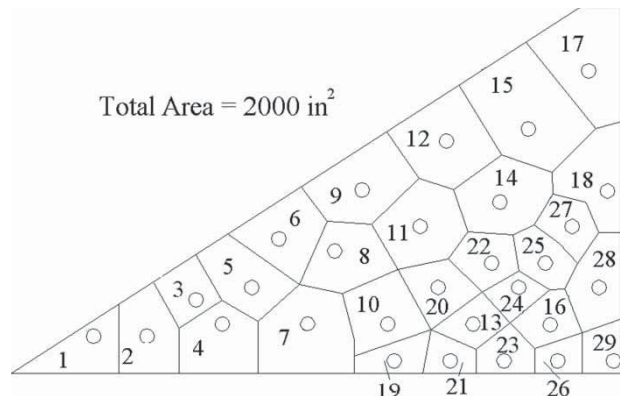


Fig. 3 Pressure port layout

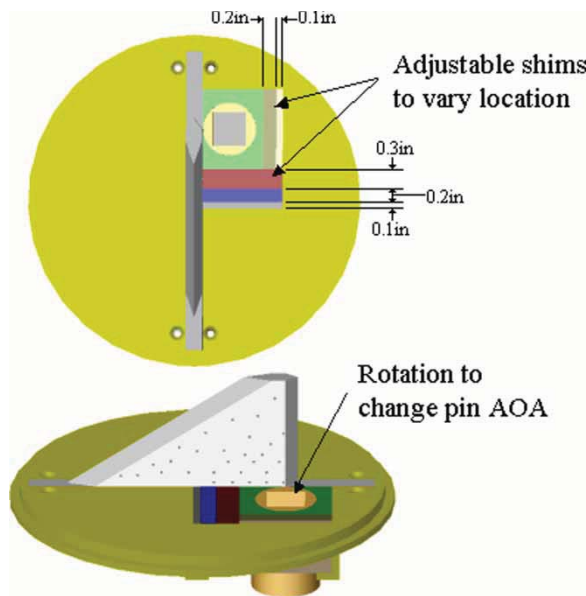


Fig. 4 Fin flat plate experimental set-up

pins could be inserted and rotated, as shown in Fig. 4. Four different pins were manufactured and tested to explore the effect of the pin geometry on the forces produced. These geometries are shown in Fig. 5.

A picture of the trapezoid pin installed next to the fin and the flat plate is shown in Fig. 6. The spacing plates and rotation mechanism for the pin can also be seen. For all of these experiments, the pin height was set to 0.5 in, which was nominally 2.5 times the longest dimension of the pin. Although some measurements were made with the fin at small angles of attack, the effect on the forces was minor and thus all of the results presented here are for a fin at 0° angle of attack relative to the freestream. Two of the pressure contours from the round pin results are shown in Figs 7 and 8 for 0.1- and 0.2-in diameter round pins, respectively. It is interesting to note that the peak pressure amplitudes are greater for the smaller diameter pin, as shown in Fig. 7, even though the overall or integrated pressure force on the fin is 50 per cent higher for the larger pin. This typifies the result that a larger area of influence on the fin is of greater importance than the magnitude of the pressure, as exemplified in Fig. 8.

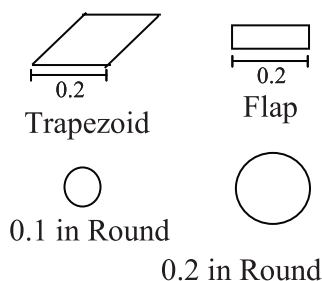


Fig. 5 Pin shapes (dimensions in inches)

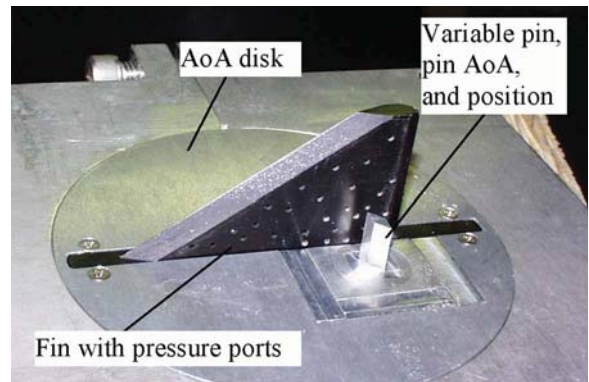


Fig. 6 Experimental set-up for pin shape and optimization of pin location testing

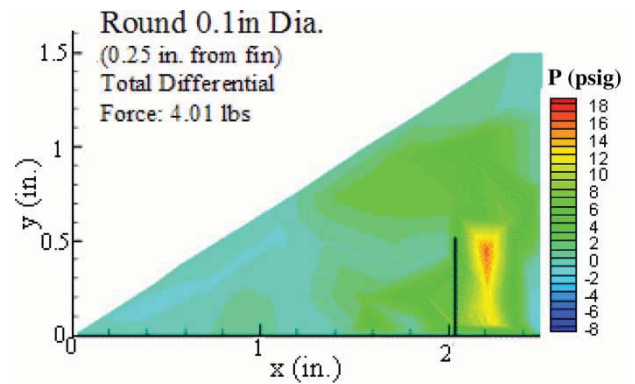


Fig. 7 Fin pressure induced by 0.1 in diameter, 0.5 in height round pin at 0.6 in from TE

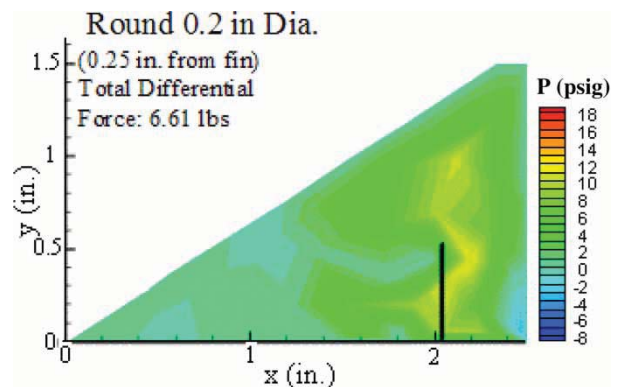


Fig. 8 Fin pressure induced by 0.2 in diameter, 0.5 in height round pin at 0.6 in from TE

Detailed studies on the optimal location and angle of the non-round pins were performed. The effect of the angle of attack of the pin on the fin side force for both the flat and trapezoidal pins was measured over a range of angles. For these measurements, 0° angle of attack represented the case where the pin was oriented, as shown in Fig. 5, and the flow was moving from the top to the bottom of the page. For positive angle of attack, the pin was rotated counterclockwise.

Figure 9 shows the effect of pin orientation on the pressure force exerted on the fin. The pin orientation does not have a very strong effect on the flat pin, whereas for the trapezoidal pin the force can vary by a factor of two, depending on the orientation of the pin. (Unfortunately, the trapezoidal pin failed and the full test matrix was not achieved.) Effectively, the rotation of the pin resulted in a change in the pin frontal area presented to the flow. Further research presented in detail in reference [7] demonstrated that it is this frontal area that drives the flow disturbance, which in turn drives the amount of force produced on the fin. For both the pins, an angle of attack of -30° was near the peak presented area and thus the best orientation tested for force generation. This pin orientation was used for the remaining tests to optimize the pin location.

Previous efforts had demonstrated [5] that the force level was increased as the pin was moved closer to the trailing edge of the fin. This increase in force was found to be due to the fact that the low-pressure region found downstream of the pin would occur off the body. Since similar results were expected for the non-round pins, the search range for the optimal pin location was narrowed. In Fig. 10, the force levels for the round pins (prior results), trapezoidal, and flat pins are shown as a function of distance from the fin trailing edge for a fixed pin height and separation distance from the fin. While the optimal location appears to vary slightly for the flat pin and the trapezoidal pin, in both cases it is near 0.65 in from the trailing edge. It is possible that this is also the optimal location for the round pin as well, though the data are too coarse to be conclusive.

The separation distance of the flat pin from the fin was found to strongly affect the force generated. As seen in Fig. 11, the force levels varied by a factor of

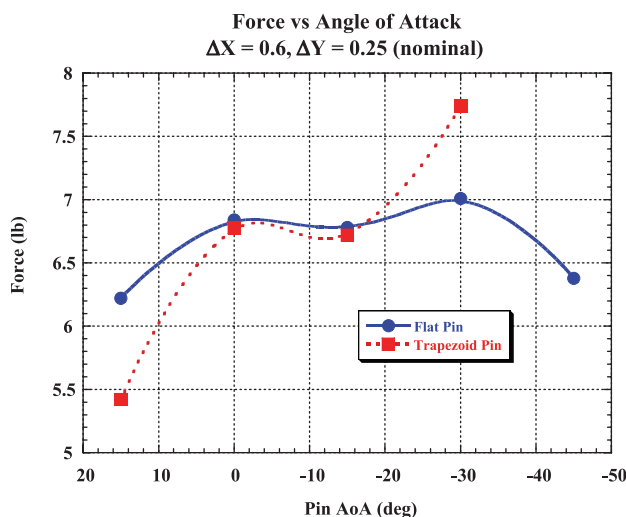


Fig. 9 Effect of pin angle of attack on the pressure force generated on the fin

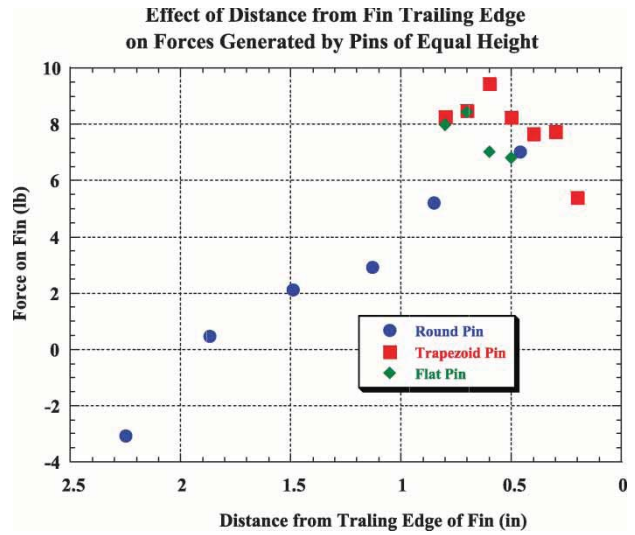


Fig. 10 Effect of distance from the trailing edge on force produced by the pins

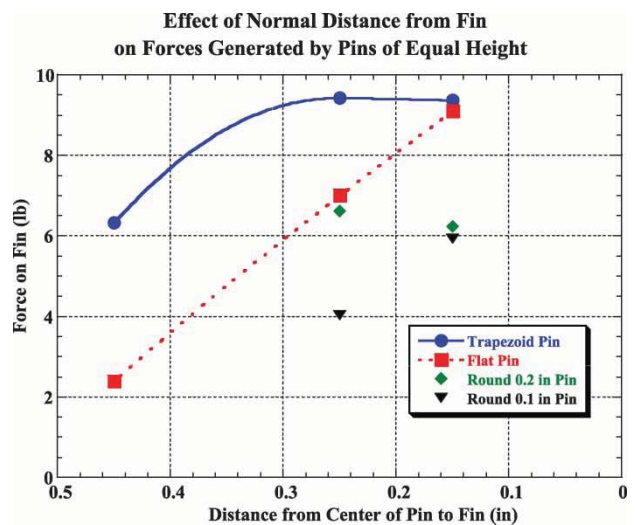


Fig. 11 Effect of distance from the fin on force generated by various pins

four for the flat pin. For the trapezoidal pin, the force induced on the fin did not change noticeably as the pin was moved from 0.15 in from the fin to 0.25 in; however, it rolled off rapidly for further separation. For the flat pin, there was a noticeable change in both the total forces and the pressure contours as the pin was moved perpendicularly away from the fin. In Fig. 12, the flat pin is 0.25 in from the fin, while in Fig. 13, the pin has been moved closer to 0.15 in.

These experiments, which tested a pin in proximity to a fin on a flat plate, demonstrated that the force level produced by pins could be augmented by appropriate placement and orientation of a non-round pin. The use of non-round pins resulted in force levels that were 50 per cent higher than that for round pins. It was also shown that the streamwise location of a pin

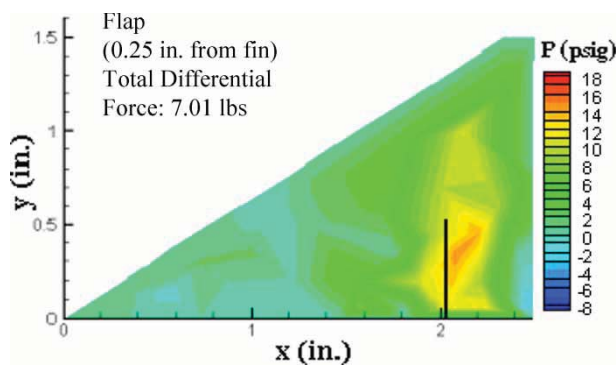


Fig. 12 Fin differential pressure induced by 0.5 in height flat pin at 0.6 in from TE

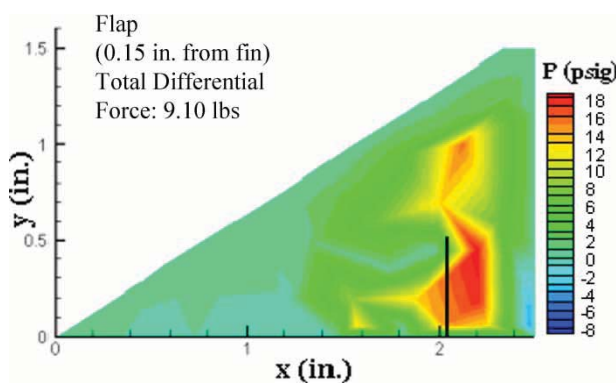


Fig. 13 Fin differential pressure induced by 0.5 in height flat pin at 0.6 in from TE

for maximum force generation was independent of the geometries tested. The results demonstrated that the force levels had a strong dependence on the separation between the pin and the fin. There was some evidence that the force levels were reduced as portions of the pin entered the boundary layer of the fin. The orientation of the pins was also shown by the experiments to introduce changes in the force level on the fin. A third set of experiments involving a flat plate and a fin were conducted using a force balance and a further refined set of pins, as described by Hay and Massey [7]. The experimental results were very useful in optimizing the location of the pins; however, they were lacking in predicting the total forces and moments that would be developed on a projectile. For that reason, computational studies were conducted.

3 CFD OF PINS AND COMPARISON TO SUBCALIBER RANGE TESTS

CFD simulations were completed using CFD++ (Metacomp Technologies, 2000) to obtain force and moment data for the projectiles over a range of supersonic Mach numbers. CFD++ solves the Reynolds-averaged Navier–Stokes equations within a finite-volume framework. The pointwise $k-\varepsilon$

turbulence model [8] was used for the computation of the turbulent flow. Spatial discretization is second order and is accomplished using the cell centroidal values (approximately equivalent to the cell averages). The point-implicit integration scheme was used to solve the steady-state simulation.

A theoretical full-scale 50-mm projectile with a tapered leading and trailing fin edge and sharp nose tip was modelled (Fig. 14(a)). To determine the effect of the control pins on the drag coefficient, simulations were completed on three geometries: a projectile with no control pins (baseline), a projectile with diametrically opposed rectangular control pins, and a projectile with diametrically opposed parallelogram-shaped (trapezoidal) control pins (Fig. 14(b)). These control pins were turned at a 30° angle and placed parallel to the fins. The shapes and placement of the pin correspond to the results of the wind-tunnel optimization experiment discussed in section 2.

The numerical grids for each of these geometries were supplied by Metacomp Technologies under contract from GTRI. Each grid was unstructured, contained mostly hexahedral cells, with a small number of triangular prisms, and contained ~ 2.9 million cells. Approximately 360 circumferential cells (not evenly distributed) were used to resolve the body, with 18 cells across the leading edge of each fin and sufficient clustering of the circumferential cells around the pins. Wall function spacing was used on the body, fins, and pins to limit the total number of cells needed.

The far-field boundary condition was set to allow the solver to determine the conditions at the far-field boundary (inflow, subsonic outflow, or supersonic outflow) and either explicitly sets the boundary condition to free-stream conditions (inflow and subsonic outflow) or extrapolates as necessary (supersonic outflow). Free-stream pressure and temperature are set to standard sea-level conditions (i.e. 101.325 kPa and 288.15 K, respectively). Density is then calculated from the perfect gas assumption. For the projectile body, fins, and control pins, the boundary condition is set to be a no-slip, adiabatic wall.

The CFD simulations were completed at velocities between Mach 1.5 and 4.0 to ensure data overlap with previously obtained range data for a subscale round fired from a rifled barrel (R. Whyte, W. Hathaway, and M. Steinhoff, 2008, personal communication). The CFD data were also needed to augment this experimental data for use in the 6-DOF simulations as the

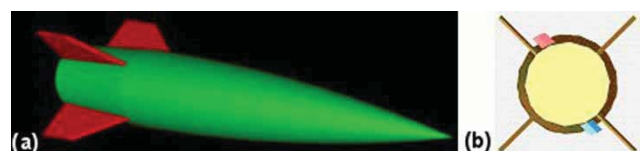


Fig. 14 (a) Three-dimensional rendering of baseline CFD model and (b) aft view of pins

increase in drag due to the presence of the control pins and the roll torque created by the control pins was not adequately measured in the wind tunnel tests.

The drag was determined directly from the axial force coefficient, C_{X0} , and the roll torque directly from the axial moment. The presence of the control pins increased the drag over the entire range of Mach numbers, as expected (Fig. 15). At a given Mach number, the increase in drag due to the presence of the control pins decreased with increasing Mach numbers. Figure 16 shows the surface pressure contours for the projectile with rectangular cross-section control pins. The areas of high pressure on the fins near the control pins cause the roll torque development. Figure 17 shows that the roll torque coefficient ($C_{l\delta}$) decreased

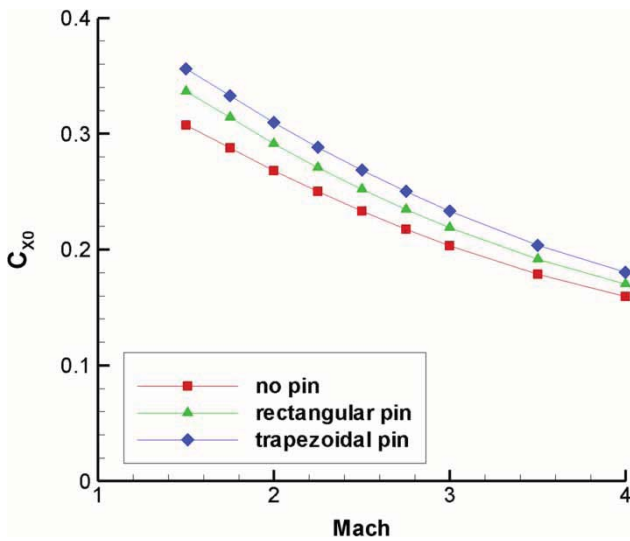


Fig. 15 Computed axial force coefficient versus Mach number

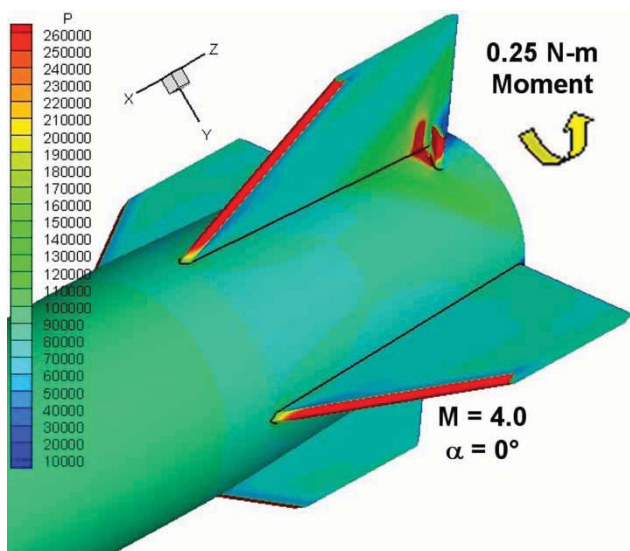


Fig. 16 Surface pressure contours, blind CFD

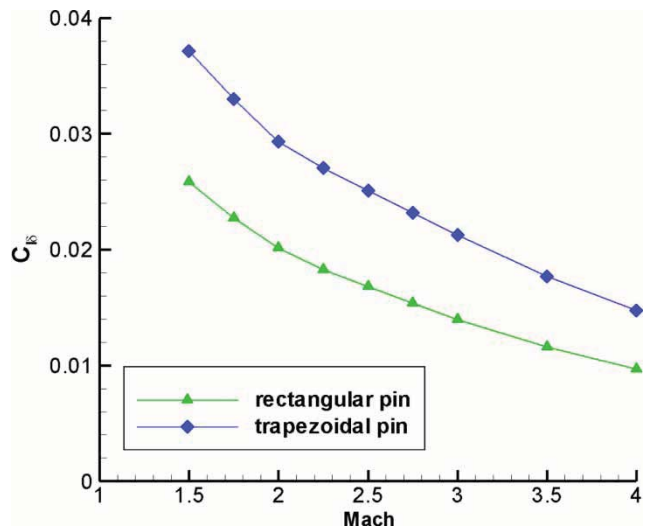


Fig. 17 Computed roll torque coefficient versus Mach number

by almost 75 per cent over the range of Mach numbers investigated. The trapezoidal control pin created substantially more roll torque over the entire range of Mach numbers, as expected.

Because the CFD was underway prior to developing the model for the range test, the cylindrical pins ultimately used in the subscale range test were not modelled. After completing the CFD for both the rectangular pin and the trapezoidal pin configurations, it was believed that the rectangular pin data would likely be more in line with that of the cylindrical control pins in the planned subscale range test. Hence, the aerodynamic coefficients from the rifled range test (R. Whyte, W. Hathaway, and M. Steinhoff, 2008, personal communication) were modified by the CFD results of the rectangular control pins. The effect of these differences on the estimates will be addressed in a later section.

Six-DOF simulations were completed using the augmented experimental data at Mach 2.0, 2.5, and 3.0. These Mach numbers were chosen to correspond to the Mach numbers of the planned subscale range test. The results of the 6-DOF simulations showed that the projectile could be expected to complete 8–10 turns during the flight down-range depending on the Mach number.

3.1 Aerodynamic experimental facility range tests

After completion of the 6-DOF simulations, subscale flight hardware was designed and built. The baseline projectile was a 25-mm subscale projectile with blunt fin leading and trailing edges, a relatively large fillet between the fins and the body, and a blunt nose tip (Fig. 18). A steel spin pin was inserted into the projectile base to determine the projectile roll position during analysis. The roll torque models (Fig. 18(b)) were created using a control pin of circular cross-section

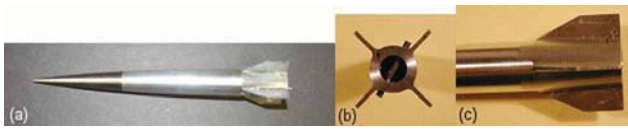


Fig. 18 Photo of short pin model (a) complete projectile, (b) base view, and (c) close-up of fins

rather than that of the optimized parallelogram shape investigated in the computer simulations to ease machining requirements (and control costs) on a proof of concept experiment. The cylindrical control pins were constructed of 1/16th-in diameter drill rod and machined to 15.0 and 16.7 mm in length to produce the 1.78-mm short control pin model and the 2.54-mm long control pin model, respectively. A hole was drilled through the body to allow for the correct placement of the diametrically opposed control pins (~ 2.79 mm from the projectile base and a 16° rotation from the fin). The chosen rod was fit through the predrilled hole and centred to create two equal length control pins.

To complete the range test, the projectile was encased in a sabot system for launch. The sabot system consisted of four sabot petals, the pusher, and the obturator (Fig. 19). The four sabot petals and the obturator/pusher cup were manufactured from nylon. The pusher was manufactured from 17-4 stainless steel. Each of the four sabot petals had two slots cut out for the fins and control pins. The petals were internally contoured to the projectile shape and fit together to create a cylinder. The pusher cup accommodated the pusher, the sabot petals, and the projectile. The exterior diameter of the pusher cup was flared near the base for an interference fit with the barrel. This allowed for a consistent velocity to be maintained for the charge weight utilized. The total package weight (projectile and sabot system) was ~ 120 g.

The projectiles were fired from a modified, smooth bore, 25-mm Bushmaster Mann barrel through the range at the US Army Research Laboratory (ARL) Aerodynamic Experimental Facility (AEF). The ARL AEF

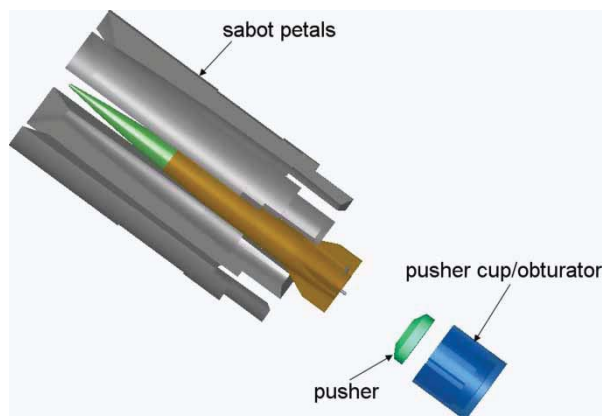


Fig. 19 Exploded three-dimensional rendering of the sabot system with projectile

was designed to evaluate the complete aeroballistics of projectiles as described by Braun [9]. Up to six high power, orthogonal x-rays were utilized to determine the structural integrity and launch dynamics of the projectile in a manner consistent with other programs (Plostins *et al.* [10], Plostins *et al.* [11], and Bornstein *et al.* [12]). The range facility itself consists of 39 orthogonal spark shadowgraph stations (Fig. 20) arranged in five groups over a trajectory length of 100 m. Each station provides a vertical and horizontal direct shadow image of the passing projectile at a known time. From these images, the raw data (i.e. the spatial coordinates and angular orientation of the projectile relative to the earth fixed range coordinate system as a function of the spark time) can be obtained.

The raw data are processed with ARFDAS [13] to determine the aerodynamic coefficients and derivatives. ARFDAS incorporates a standard linear theory analysis and a 6-DOF numerical integration technique. The 6-DOF routine incorporates the maximum likelihood method (MLM) to match the theoretical trajectory to the experimentally measured trajectory. The MLM is an iterative procedure that adjusts the aerodynamic coefficients to maximize a likelihood function. Each projectile fired was initially analysed separately (single fits), and then combined in appropriate groups for simultaneous analysis using the multiple fit capability. The multiple fit approach provided a more complete spectrum of angular and translational motions than would be available from any single trajectory.

Up to three Mach numbers were investigated for each configuration for a total of 15 shots. For the baseline configuration, one projectile was shot for each nominal Mach numbers of 2.0, 2.5, and 3.0. For the short pin model, three projectiles were shot for each nominal Mach numbers of 2.0, 2.5, and 3.0. For the long pin model, three projectiles were shot for the nominal Mach number of 3.0.



Fig. 20 Photo of dual plane (orthogonal) spark shadowgraph stations with infrared sensor triggers and spark source

Gun launch was successful: consistent velocities were obtained and the sabot petals cleanly separated upon muzzle exit; there was no interference with the projectile motion and structural integrity of the projectile was maintained. Horizontal and vertical shadowgraph photographs were obtained at each station for each shot. Thus, all aerodynamic coefficients were obtained for each shot. Only the results of C_{X0} and $C_{l\delta}$, and the resulting travel down-range are presented here for brevity and comparison with CFD. The reader is referred to Silton [14] for the remaining aerodynamic coefficients.

C_{X0} decreased nearly linearly with Mach number for both baseline and short pin configurations (Fig. 21). For a given Mach number, C_{X0} increased with the introduction of the control pin as well as with pin length. The diametrically opposed control pins created roll torque as expected (Fig. 22). The non-zero $C_{l\delta}$ for the

baseline case can be accounted for small asymmetries due to the spin pin. For the short pin geometry, $C_{l\delta}$ does not significantly vary with Mach number unlike the other aerodynamic coefficients. At Mach 3, the 50 per cent increase in control pin length nearly doubled the roll torque coefficient. This indicates that there would be a much faster response from the projectile.

The roll rate increased as the projectile travelled down-range. Comparing shadowgraphs at adjacent stations when the roll rate is small (Fig. 23) and further down-range when a larger roll rate has been achieved (Fig. 24), the difference is quite noticeable. The spin pin has barely moved between Figs 23(a) and (b), where the round travelled from 6.7 to 8.2 m. At least a 90° rotation was achieved between Figs 24(a) and (b), where the round travelled from 90 to 91.4 m. Although not shown here, the difference in Mach number does not effect the roll rate much. The increase in pin length, however, more than doubles the roll rate by the end of the range.

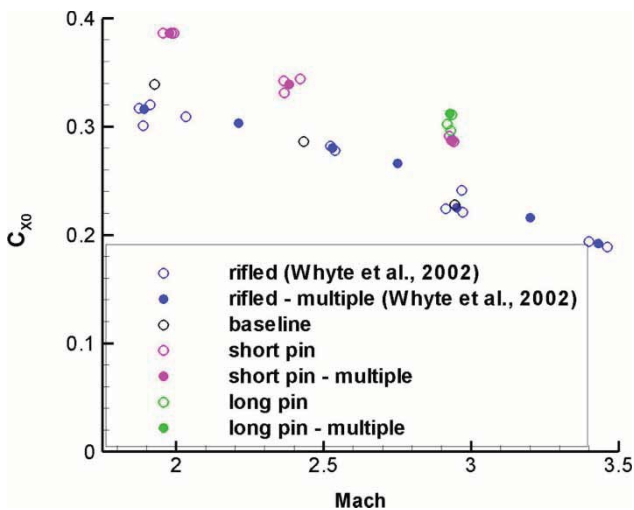


Fig. 21 Experimental zero-yaw axial force coefficient as a function of Mach number

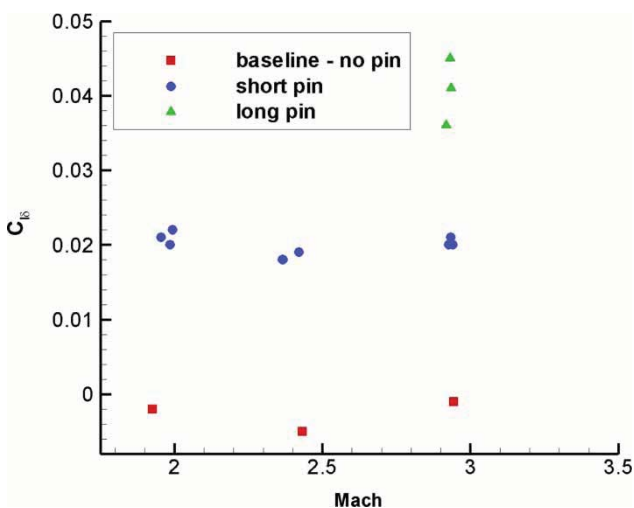


Fig. 22 Experimental roll torque coefficient as a function of Mach number

3.2 Computational and range test comparisons for subscale model

In this subsection, the results of the range test are compared to:

- (a) CFD and 6-DOF simulations;
- (b) 6-DOF simulations using updated aerodynamics coefficients;
- (c) CFD results using matched physical and atmospheric conditions.

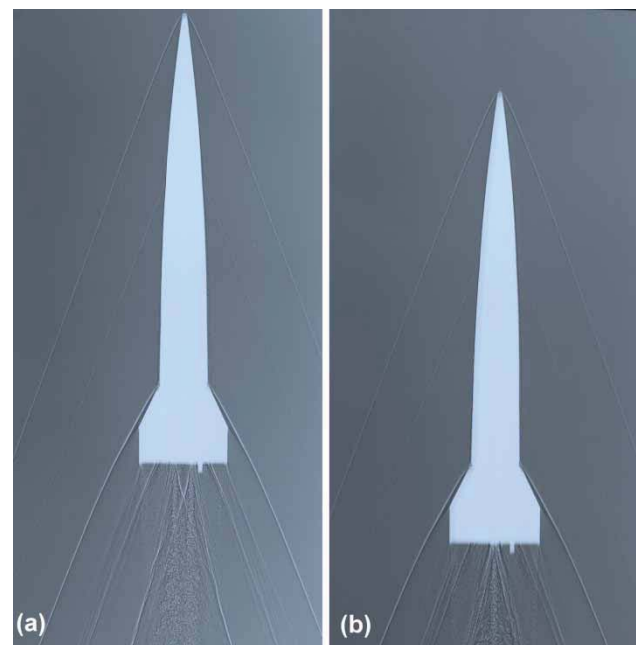


Fig. 23 Vertical shadowgraphs for shot 24 096 at stations (a) 22 and (b) 27

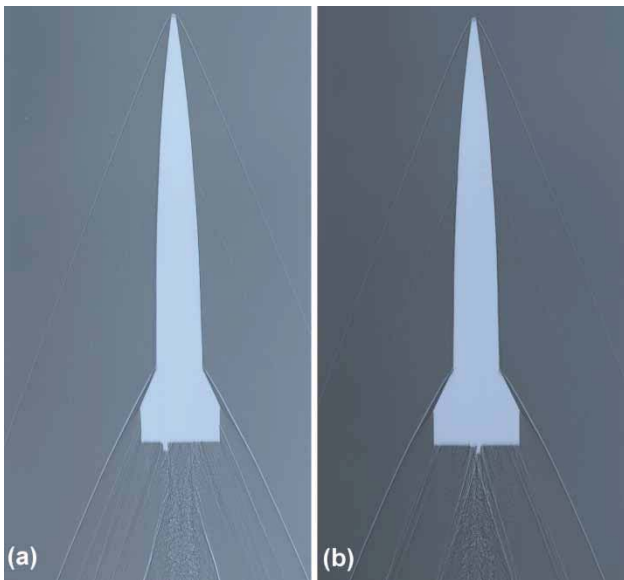


Fig. 24 Horizontal shadowgraphs for shot 24 096 at stations (a) 295 and (b) 300

3.3 CFD and 6-DOF

This comparison was completed in order to determine how well the CFD and 6-DOF simulations predicted the range test results despite differences in the geometric model. The differences were not just model size, but also fin leading and trailing edge taper (tapered versus blunt), nose bluntness (sharp versus blunt) and control pin shape (rectangular versus cylindrical), and relative orientation (parallel versus radial to the fin). Also, the 6-DOF simulations assumed aerodynamic coefficients determined for the baseline projectile shot from a rifled gun tube (R. Whyte, W. Hathaway, and M. Steinhoff, 2008, personal communication). A larger C_{X0} is expected for the range test due to the bluntness of the fins and the nose tip. Nonetheless, CFD does a reasonable job of predicting C_{X0} (Fig. 25). CFD underpredicts the increase in C_{X0} due to the presence of the control pin due to the difference in pin shape. However, augmenting the rifled range test data by this difference produces a fair estimate of C_{X0} for the short pin projectile.

CFD does well predicting $C_{l\delta}$ despite modelling rectangular, rather than the experimental cylindrical pins (Fig. 26). The predictions are quite good at Mach 2.0 and 2.5, leading one to believe that the differences in control pin shape are insignificant at these Mach numbers. Perhaps, the three-dimensional relieving effects are as significant for the rectangular pins turned at a 30° angle and parallel to the fins as for the symmetrically placed circular pins. At Mach 3.0, $C_{l\delta}$ is noticeably underpredicted, indicating that geometric differences and pin placement become important at higher Mach numbers.

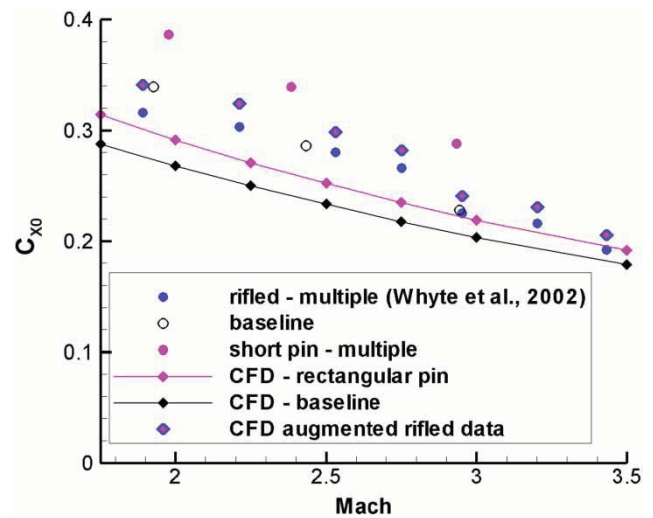


Fig. 25 Axial force coefficient comparison between the range test and blind CFD

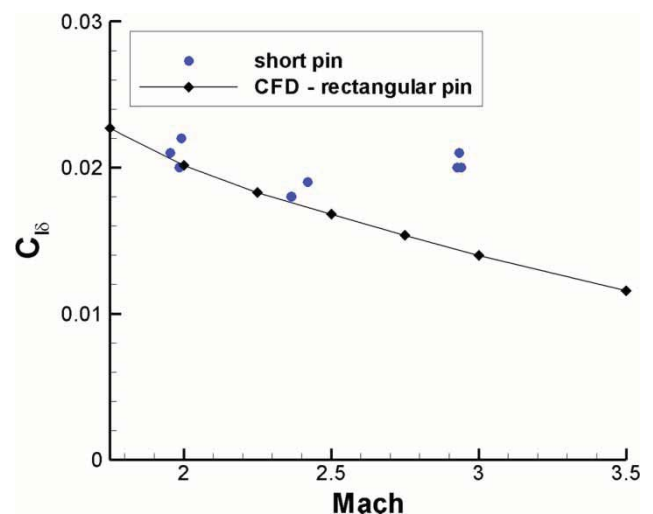


Fig. 26 Roll torque coefficient comparison between the range test and blind CFD

As there were differences between the axial force and roll torque coefficients used for the 6-DOF simulation and the values determined by the range test, one expects there to be corresponding differences in the results. This was indeed the case as the number of revolutions achieved at Mach 3.0 was underpredicted at 90 m (8.7 versus 7.3), whereas the number of revolutions at the lower Mach numbers was overpredicted at 90 m (6.8 versus 7.9 at Mach 2.5 and 7.0 versus 8.5 at Mach 2.0). Regardless, the 6-DOF simulations provided a good idea of what could be expected to occur during the range tests, indicating that the models do not have to include the exact geometry for the first approximations.

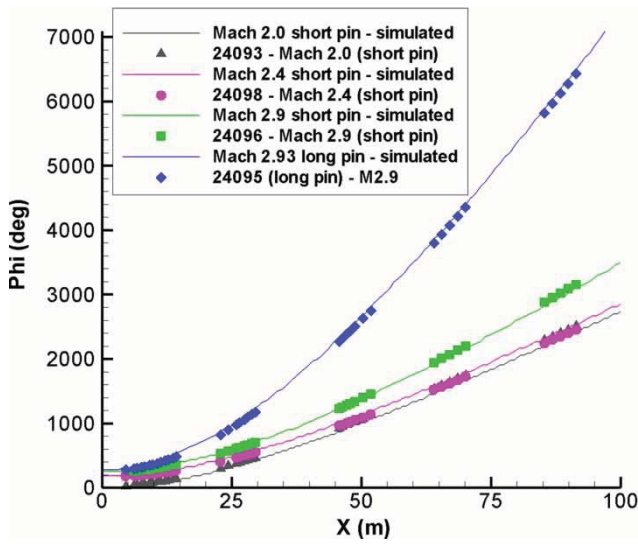


Fig. 27 Comparison of updated 6-DOF and range test results for projectile rotation as a function of distance

3.4 Updated 6-DOF

After completion of the range tests, the 6-DOF simulations were repeated using the aerodynamic coefficients obtained from the range test to populate the database. Very good agreement in both roll rate and, hence, number of revolutions was achieved (Fig. 27), indicating that accurate 6-DOF simulations can be obtained if an accurate aerodynamic coefficient database is available. This validates the 6-DOF simulations.

3.5 Updated CFD using accurate geometry and flow conditions

After completion of the range tests, two new sets of CFD calculations were completed under contract by Metacomp Technologies using the short cylindrical pin model and the long cylindrical pin model. Each computation was completed at 0° angle of attack and exactly matched the test conditions of the multiple fit range results for the model, allowing for direct comparison of C_{X0} and $C_{l\delta}$.

CFD accurately determined C_{X0} at all the three Mach numbers for both model configurations (Fig. 28). CFD did not do quite as well predicting $C_{l\delta}$ (Fig. 29). It predicted a continuous decrease for the short pin model. The range test, however, showed a small decrease in $C_{l\delta}$ between Mach 2.0 and 2.5 with a subsequent increase between Mach 2.5 and 3.0. However, both of these changes are small and the differences could be due to round- to-round machining variations and/or slight differences in the geometry of the fired rounds and the computational model. For the long pin model, the CFD underpredicts $C_{l\delta}$. The scatter in the range test results for the long pin model (known to 1 per

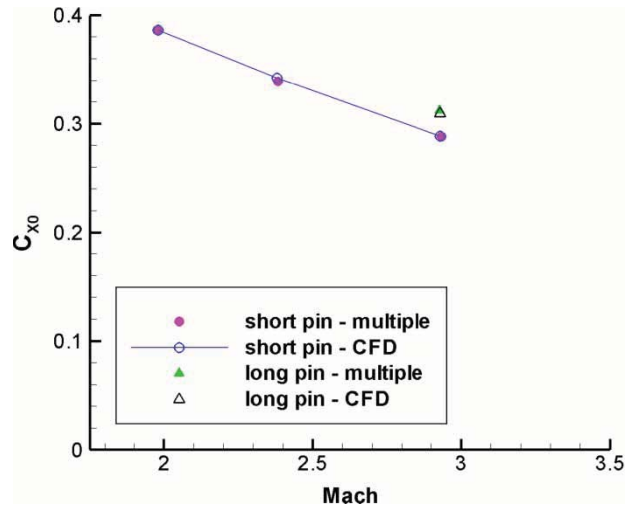


Fig. 28 Comparison of updated CFD to range test zero-yaw axial force coefficient

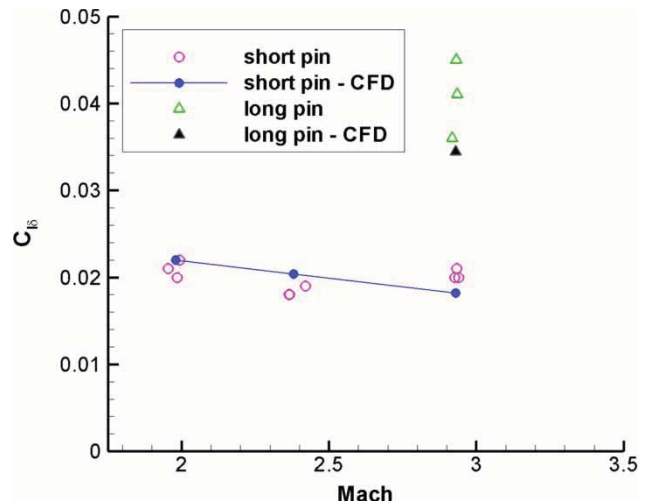


Fig. 29 Comparison of updated CFD to range test roll torque coefficient

cent) is too large to be attributed to an angle-of-attack dependency considering the small variation in angle of attack. Therefore, the scatter is more likely due to round-to-round geometric differences including variations in pin lengths or slight changes in pin angle relative to the fins, causing $C_{l\delta}$ to vary.

From CFD visualization, it is possible to see the forces created by the pins on the fins that are responsible for the roll torque (Figs 30 and 31). If one also compares the shock structure predicted by the CFD (Fig. 32) to that seen in the range (Fig. 33), the similarities are easily noticeable. The small differences in the base flow are likely a result of differences in roll orientation, and hence the location of the control pin. Based on the comparison of the updated CFD results to the range data, CFD should be able to predict the forces produced by the control pins as the problem

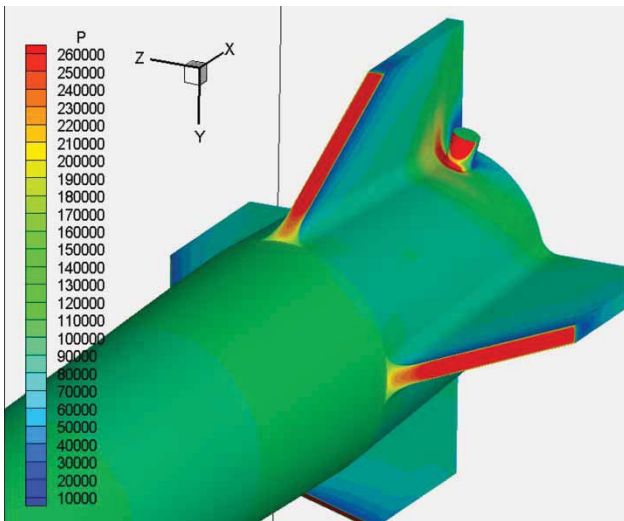


Fig. 30 Surface pressure contours for updated CFD on short pin model at Mach 2.93

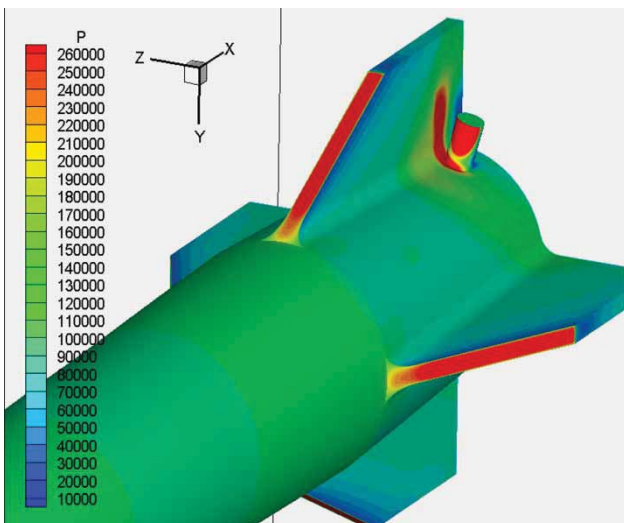


Fig. 31 Surface pressure contours for updated CFD on long pin model at Mach 2.93

is varied (i.e. changes in pin shape, pin location, and free-stream Mach number).

4 TRANSONIC EXPERIMENTAL FACILITY SPARK RANGE TESTS

After the subscale firings and CFD were complete, a full-scale range test was developed to test the control authority of the control pins in the divert configuration. The first test fires of the assembled projectile and sabot were performed at the outdoor 700 ft Site at the ARL Transonic Experimental Facility (TEF). These test firings served primarily as a shakedown test to ensure that only the bullet flies down-range, that the non-divert projectiles flies straight, and that

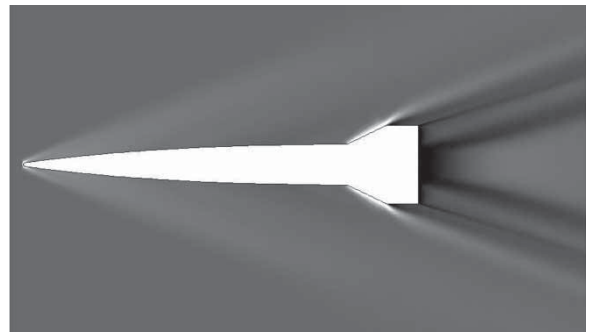


Fig. 32 Pressure coefficient contours through fin symmetry plane for short pin model at Mach 2.93

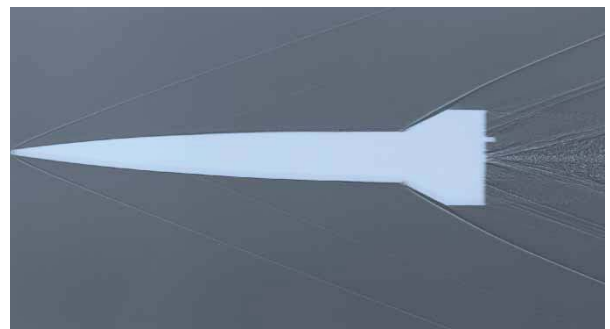


Fig. 33 Shadowgraph at station 27 for short pin model at Mach 2.93

the divert projectiles would stay within the indoor spark range without damaging the equipment. This was done to ensure that the shadowgraph equipment and the building of the TEF did not suffer severe damage from errant projectiles or sabots. Additionally, the first set of firings was used to determine the charge weight required for the desired muzzle velocity and to verify that the sabot separation was clean. Although it was planned to measure the projectile flight path and orientation in the spark range, yaw cards were set up at various stations down-range of the gun during these initial tests to gain some insight into the path of the projectile. In addition to demonstrating that the projectile flew true and that none of the sabot packages would enter the range, the yaw cards also provided a preliminary indication that the pins were in fact deploying.

The launch package consisted of four sabot petals, the projectile, a pusher plate, and a pusher cup. The unassembled parts are shown in Fig. 34 and a partially assembled launch package along with a fully assembled launch package is shown in Fig. 35.

After assembly, the launch package was breech loaded into the 75-mm smooth-bore gun, shown in Fig. 36. The gun fired a single projectile at a nominal muzzle velocity of 1450 m/s. A radar system was used to measure the exit velocity of each round. Down-bore photography was acquired as well as the muzzle

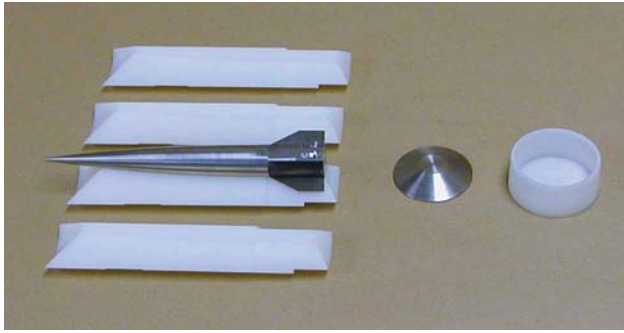


Fig. 34 Projectile, sabot petals, pusher plate, and cup before assembly



Fig. 35 Partial and complete assembly of launch package

chamber pressure. This information was used to verify that the launch package remained intact inside the gun tube and that over pressurization did not occur. A Hadland digital camera and x-ray stations were located a few meters from the exit of the gun, and the frame for these stations and the first x-ray unit can be seen on the far left of Fig. 36. The digital camera and x-rays were instrumental in determining

whether there was a clean separation between the projectile and the sabot, and to ensure that the projectile remained intact. Further down-range, wooden 2×4 's were set up to mount the yaw cards, which consisted of either black roofing paper or cardboard. The yaw card mounts as well as the target and the embankment into which the projectile was fired are shown in Fig. 37.

During the shakedown firings, several problems were discovered and remedied. A small number of rounds were then fired with guidance pins that were designed to deploy after launch. Although mostly qualitative, the holes punched in the yaw cards by the projectile provided a clear indication that the projectile diverted downward, which thus indicated that the pins had been deployed. A collage of four different yaw cards at different down-range distances is shown in Fig. 38, where the drop is clearly noticed and one can even see additional holes produced by the pins particularly on the 9.1-m yaw card. With these successful test fires, the test program was cleared to move into the indoor spark range.

Another range at the ARL TEF is the indoor spark range that allows for the aerodynamics of larger caliber projectiles to be determined. Figure 39 shows an inside view of the spark range, looking up-range towards the projectile entrance. The spark range provides pairs of orthogonal shadowgraphs at 25 stations, with five groups containing five stations each. The shadowgraph pictures are read and are reduced to obtain the aerodynamic performance of the projectile. By comparing the results with and without the control pins, the effect of the control pins can be determined.

The station ranges are identified with a two-digit number. The first digit indicates the group to which the station belongs, and the second digit indicates the station within that particular group. Side view shadowgraphs are obtained from exposed film plates mounted on the left wall of the facility (i.e. viewing projectile from left of the line-of-fire) and are designated with 'W'. Bottom view shadowgraphs are obtained from exposed film plates mounted in pits in the floor of the facility (i.e. viewing projectile from beneath the line of fire) and are designated with 'P'. For example, station 23W is the wall shadowgraph from the third station in



Fig. 36 A 75-mm gun used to launch projectiles at ARL



Fig. 37 Stations for yaw cards and target on a 700-ft range

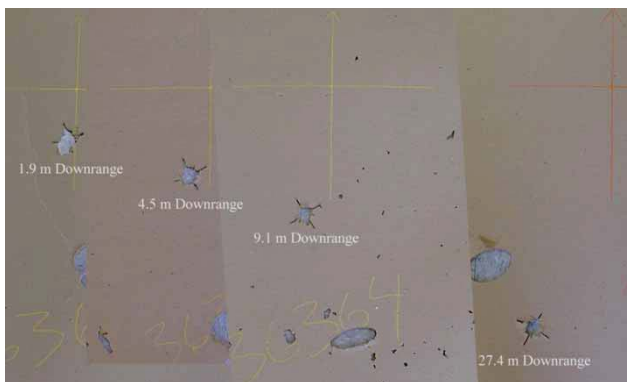


Fig. 38 Composite picture of four down-range yaw cards showing divert of projectile

the second pit (i.e. the 8th of 25 stations), and station 51P is the pit shadowgraph from the first station of the fifth pit (i.e. the 21st of the 25 stations).

Table 1 shows the spark range coordinate of each shadowgraph station. The spark range coordinate system origin is located inside the spark range near the first spark station, as shown in the table. The spark range coordinate system is typically aligned with the gun range coordinate system to within several milliradians, but the gun range coordinate origin is located at the gun muzzle. For this test, the muzzle was located at a spark range coordinate of -39.45 m (-129.44 ft). Approximately 200 m of the flight trajectory are captured via spark photography. The anticipated trajectory of the divert rounds was modelled using a 6-DOF simulation and the forces generated by the pins, which were estimated from the prior CFD and experimental studies. This nominal trajectory is superimposed on a layout of the spark range in Fig. 40, including the location of the gun relative to the first set of shadowgraphs and the expected deployment of the pins.

The results from the spark range tests clearly showed the effectiveness of the guidance pins as a means to divert the projectile. Selected shadowgraphs from a single divert test have been aligned and assembled in Fig. 41. In these pictures, the rapid drop of the projectile of roughly 1 m over 150 m of travel can easily



Fig. 39 ARL TEF spark range

be seen. This path is reasonably close to that predicted; however, the pins appeared to deploy sooner than expected. It can also be seen in the photographs that the projectile is undergoing an oscillatory pitch, which was also predicted by the 6-DOF analysis prior to launch.

Trajectories were fit to the projectile position data read from the spark range shadowgraphs for both divert rounds and non-divert rounds. A comparison of two of these trajectories is shown in Fig. 42 for the vertical plane, and Fig. 43 for the horizontal plane. For the divert shot shown in Fig. 42, shadowgraphs of the projectile were only captured in the first three groups, but this was enough to show that the divert

Table 1 Spark range coordinates for shadowgraph stations

Group 1		Group 2		Group 3		Group 4		Group 5	
Stat	Range (m)								
1-1	0.1	2-1	45.8	3-1	91.5	4-1	137.3	5-1	182.9
1-2	6.0	2-2	52.0	3-2	97.6	4-2	143.3	5-2	189.2
1-3	12.1	2-3	57.9	3-3	103.8	4-3	149.4	5-3	195.3
1-4	18.2	2-4	64.1	3-4	109.8	4-4	155.6	5-4	201.3
1-5	24.4	2-5	70.2	3-5	116.1	4-5	161.5	5-5	207.4

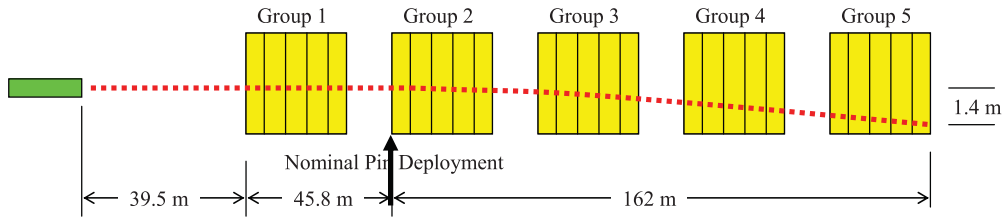


Fig. 40 Shadowgraph stations and nominal trajectory of divert round

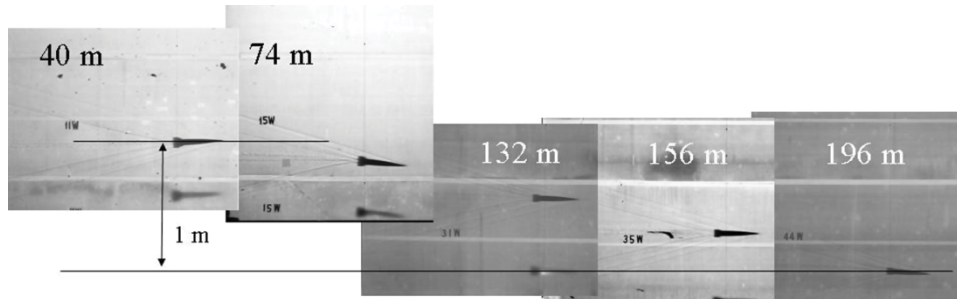


Fig. 41 Shadowgraph ensemble showing divert of projectile

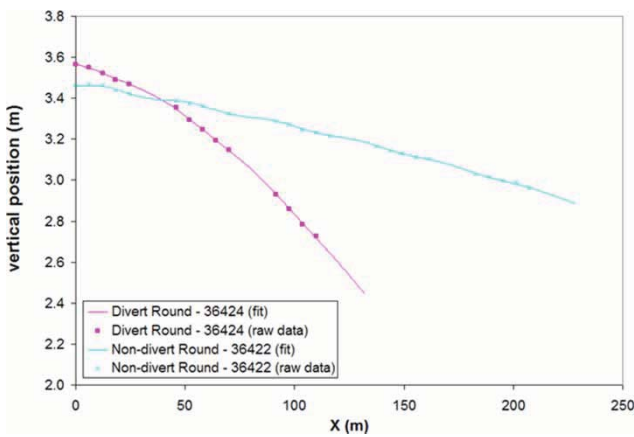


Fig. 42 Comparison of divert and non-divert round trajectories in the vertical plane

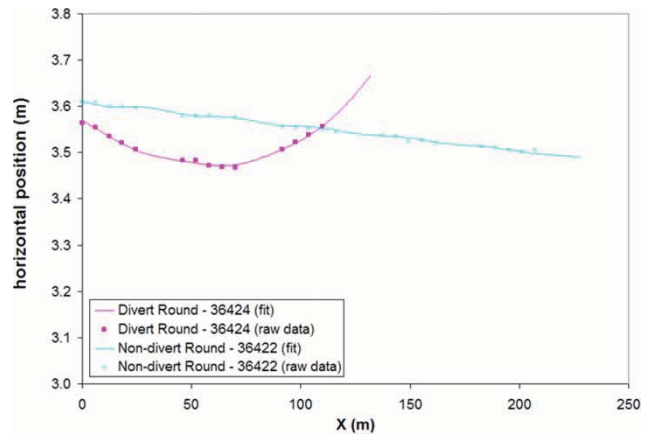


Fig. 43 Comparison of divert and non-divert round trajectories in the horizontal plane

round dropped ~0.9 m in the first 100 m of the range versus 0.3 m for the non-divert case. This equates to a vertical acceleration of 10.4 g's. In the horizontal plane (Fig. 43) the divert round was found to divert slightly to the left, indicating that a small degree of roll was introduced either as the pins deployed or as the round left the barrel. (The projectiles were loaded such that

they would divert down.) This lateral motion was much smaller than that in the vertical plane, with a net travel on the order of 0.2 m in the first 100 m of the range. This divert resulted in a change in the direction of the flight and thus the projectile experienced 9.4 g's of acceleration in the horizontal plane. A vector summation of the horizontal and vertical accelerations equates to a

total acceleration of ~ 14 g's experienced by the projectile. This is quite large considering that this was an extremely stable test projectile (1.5 caliber static margin). This indicates that an 80 N force was induced by the guidance pins, which is quite a large force for the small guidance pins.

The factors that determine whether a guided projectile can intercept a moving target depend on many factors beyond the amount of steering force generated, such as the manoeuvrability of the target, closing rate, and the navigation ratio. Typically the manoeuvrability of the interceptor needs to be three times the target manoeuvrability [15]. Given that the projectile as tested was made more stable than a tactical round, in order to ensure range safety, it would be reasonable to assume that higher accelerations could be achieved and that the guided projectile could even intercept targets undergoing evasive manoeuvres of 10–15 g's.

5 CONCLUSIONS

The tests in TEF were a success and allowed us to quantitatively measure the turning forces developed on a full-scale projectile travelling at speeds in excess of Mach 4. They also served to demonstrate that the mechanical actuation of the guidance pins was a practical reality as the pins were repeatedly deployed. Further, the predictive analysis and years of testing leading up to this test were validated, clearly demonstrating that combinations of wind tunnel tests, CFD, 6-DOF, FEA, shock testing, and so on, when used properly, can be used to successfully design a guided projectile that behaves as expected. For example, the predicted divert of the test round, as shown in Fig. 40, of 1.4 m over 160 m compares quite favourably to the measured divert, shown in Fig. 42, where ~ 1.4 m of divert would be seen if the trajectory was extended to 160 m. The careful application of experimental methods and CFD served to reduce the number of test articles that are needed to be fired in order to prove the concept. This led to a reduction in the total cost to the program and a greater understanding of the aerodynamics involved.

Through appropriate placement of control pins on a projectile, sufficient control forces can be developed to manoeuvre a high-speed projectile. This validated technology has application for guiding both supersonic projectiles and missiles into manoeuvring targets and correcting for aiming errors, thus enabling a number of air defence scenarios as well as enabling new offensive capabilities.

REFERENCES

- 1 **Kandebu, S. W.** New powerplant key to missile demonstrator, *Aviation Week*, 2 September 2002.
- 2 **Smith, B. J., Nourse, R. W., Baumann, J. L., and Sanders, G.** Extended area protection system (EAPS) program overview. In Proceedings of the 2006 IEEE Aerospace Conference, 12 December 2005, IEEEAC paper no. 1069, version 4.
- 3 **Chen, M. M.** Stochastic analysis of initial extended area protection and survivability (EAPS) projectile. Army Research Laboratory Report, ARL-TR-4140, June 2007.
- 4 **Warnash, A. and Killen, A.** Low cost, high G, micro electro-mechanical (MEMS), inertial measurements unit (IMU) program. In Proceedings of the 23rd Army Science Conference, December 2002.
- 5 **Massey, K. C., McMichael, J., Warnock, T., and Hay, F.** Mechanical actuators for guidance of a supersonic projectile. In Proceedings of the 23rd Applied Aerodynamics Conference, Toronto, Ontario, Canada, AIAA paper 05-4970.
- 6 **Massey, K. C., Guthrie, K. B., and Silton, S. I.** Optimized guidance of a supersonic projectile using pin based actuators. In Proceedings of the 23rd Applied Aerodynamics Conference, Toronto, Ontario, Canada, AIAA paper 05-4966.
- 7 **Hay, F. and Massey, K. C.** Parametric investigation into the location and geometry of deployable pins used for guiding supersonic projectiles, 2005, AIAA paper 05-2-20B.
- 8 **Goldberg, U. C., Peromian, O., and Chakravarthy, S. A.** wall-distance-free K-E model with enhanced near-wall treatment. *J. Fluids Eng.*, 1998, **120**(3), 457–462.
- 9 **Braun, W. F.** The free flight aerodynamics range, BRL-R-1048. US Army Ballistic Research Laboratory, Aberdeen Proving Ground, Maryland, 1958.
- 10 **Plostins, P., Celmins, I., Bornstein, J., and Deibler, J. E.** The effect of front borerider stiffness on the launch dynamics of fin-stabilized kinetic energy ammunition, BRL-TR-3057. US Army Ballistic Research Laboratory, Aberdeen Proving Ground, Maryland, 1989.
- 11 **Plostins, P., Bornstein, J., and Celmins, I.** The effect of sabot wheelbase and positions on the launch dynamics of fin-stabilized kinetic energy ammunition, BRL-TR-3225. US Army Ballistic Research Laboratory, Aberdeen Proving Ground, Maryland, 1991.
- 12 **Bornstein, J., Celmins, I., Plostins, P., and Schmidt, E. M.** Launch dynamics of fin-stabilized projectiles. *J. Spacecr. Rockets*, 1992, **29**(2), 166–172.
- 13 **ArrowTech Associates.** ARFDAS: ballistic range data analysis system. User and technical manual, South Burlington, Vermont, 1997.
- 14 **Silton, S.** Comparison of predicted actuator performance for guidance of supersonic projectiles to measured range data. AIAA paper 2004-5195, 2004.
- 15 **Fleeman, E. L.** *Tactical missile design*, 2001 (AIAA, Reston, Virginia, USA).